Hindawi
Advances in Materials Science and Engineering
Volume 2018, Article ID 8191095, 10 pages
https://doi.org/10.1155/2018/8191095

Research Article

Template-Free Synthesis of Star-Like ZrO_2 Nanostructures and Their Application in Photocatalysis

Xue-Yu Tao,[1,2,3] **Jie Ma**,[1] **Rui-Lin Hou**,[1] **Xiang-Zhu Song**,[1] **Lin Guo**,[1] **Shi-Xiang Zhou**,[1] **Li-Tong Guo**,[1] **Zhang-Sheng Liu**,[1] **He-Liang Fan**,[1] **and Ya-Bo Zhu**[1]

[1]*School of Materials Science and Engineering, China University of Mining and Technology, Xuzhou, Jiangsu 221116, China*
[2]*Jiangsu Province Engineering Laboratory of High Efficient Energy Storage Technology and Equipments, China University of Mining and Technology, Xuzhou, Jiangsu 221116, China*
[3]*Xuzhou City Key Laboratory of High Efficient Energy Storage Technology and Equipments, China University of Mining and Technology, Xuzhou, Jiangsu 221116, China*

Correspondence should be addressed to Xue-Yu Tao; taoxueyu@cumt.edu.cn and Li-Tong Guo; guolitong810104@163.com

Received 16 March 2018; Revised 1 June 2018; Accepted 21 June 2018; Published 3 September 2018

Academic Editor: Marián Palcut

Star-like nano-ZrO_2 has been synthesized using $Zr(NO_3)_4{\cdot}5H_2O$ as zirconium source by a hydrothermal process without any template and surfactant. The structure of the as-prepared ZrO_2 powder was investigated by multiple advanced analytical methods. The results showed that CH_3COO^- and NO_3^- had great effects on the formation of star-like ZrO_2 nanostructures. The as-prepared ZrO_2 had a superior catalytic activity, and the reason for it was analyzed by UV-Vis diffuse reflectance spectroscopy. The effect of raw material ratios on the photocatalytic property of ZrO_2 was studied. The synthesized ZrO_2 showed a narrow bandgap (3.50–3.85 eV) and an excellent photocatalytic activity, and the degradation of RhB was up to nearly 100% in 30 min with this photocatalyst.

1. Introduction

Zirconia (ZrO_2) is one of the most important ceramic materials with three different phases: monoclinic stable below 1175°C, tetragonal stable at 1175–2370°C, and cubic stable at 2370–2680°C, respectively [1, 2]. Nanosized zirconia has specific optical and electrical properties which suits it for prospective applications in transparent optical devices, electrochemical capacitor electrodes, fuel cells, catalyst, and advanced ceramics [3–8]. Numerous synthetic strategies have been developed to obtain zirconia nanostructures including solution combustion synthesis [9], microwave-hydrothermal [10], sol-gel [11], spray pyrolysis [12], chemical vapour synthesis [13], and precipitation approach [14]. Among them, the hydrothermal method has attracted much attention because of its simple operation, mild experimental conditions, and high product purity. Catalytic properties of inorganic nanomaterials not only are related to their phase structure and chemical composition but also depend on their morphology [15]. The morphology of ZrO_2 has a significant effect on its properties [16–23] because it can control a variety of physical and chemical properties at the same time. For instance, with special morphology, flower-like zirconia nanomaterials [24] showed an excellent photocatalytic activity on the degradation of rhodamine B. In addition, the spinous ZrO_2 core-shell morphology [25] exhibited a superior hydrogen storage performance, reaching a hydrogen uptake of 1.521 wt.% at 298 K under 5 MPa.

Wastewater pollution has become a serious problem in many countries [26]. The removal of dyes from wastewater through heterogeneous photocatalysis has drawn an increasing attention over the last few decades. For degradation of organic pollutants, many studies on the heterogeneous photocatalysis were performed with oxide semiconductors such as TiO_2 [27], ZnO [28], Fe_2O_3 [29], ZrO_2 [30], and CuO [31] being applied. These nanomaterials showed an excellent photocatalytic activity on the degradation of

organic dyes. In recent years, ZrO_2-based materials have gained a considerable scientific and technological attention in heterogeneous catalysis. They have been used in the photodegradation of dye compound due to their high photocatalytic activity in the ultraviolet range, high thermal stability, chemical stability, low cost, nontoxicity, and environmentally friendly nature [32].

In recent years, many different approaches [17, 33–35] have been utilized to prepare zirconia nanomaterials with different morphologies using suitable templates and surfactants. For example, ZrO_2 nanowires and nanobelts were prepared by an alumina template and pyrolysis of $Zr(OH)_4$: RE particles, respectively. ZrO_2 mesopore microfibers have been prepared with a pluronic P-123 template [17]. A ZrO_2 hollow fiber membrane was successfully synthesized employing a polypropylene hollow fiber as the template, and the prepared zirconia hollow fiber was demonstrated to be a highly selective adsorbent for the phosphonic acid-containing compounds with high sensitivity [35]. Flake-like ZrO_2 nanocrystallites were prepared using cetyltrimethyl ammonium bromide (CTAB) as the surfactant, and the use of surfactant led to the formation of stabilized tetragonal ZrO_2 nanoparticles (15 nm) [21]. These studies demonstrated successful synthesis of ZrO_2 nanostructures with special morphology; however, most of these approaches required either suitable templates or surfactants to prepare ZrO_2 nanostructures and also included the removal of the template in the process. Therefore, searching for a simple but effective method to get a special morphology of ZrO_2 in the absence of template remains a challenge.

In this paper, a facile route was employed to synthesize the ZrO_2 nanostructures with $Zr(NO_3)_4{\cdot}5H_2O$ and CH_3COONa as starting materials without any template or surfactant. Starting materials $Zr(NO_3)_4{\cdot}5H_2O$ and CH_3COONa are cheap and affordable. Furthermore, $Zr(NO_3)_4{\cdot}5H_2O$ is water soluble and suitable for hydrothermal synthesis. Also NO_3^- is easy to remove from the system, which prevents the contamination of the products. CH_3COO^- anions tend to adsorb on the surface of ZrO_2 and play an important role in the formation of ZrO_2 particles with special morphology. In this work, the degradation of rhodamine B (RhB) with nanosized ZrO_2 was studied in aqueous solution. The novel nanostructure of ZrO_2 may lead to superior performance in the photodegradation of RhB.

2. Experimental

2.1. Materials. The chemicals used were of analytical grade and purchased from Aladdin Chemistry Co. Ltd. The chemicals were used as received without further purification.

2.2. Synthesis. ZrO_2 nanostructures were synthesized using the hydrothermal method. Figure 1 shows the synthesis route of nanosized ZrO_2. Typically, 0.123 g (0.0015 mol) of CH_3COONa was added into the solution of $Zr(NO_3)_4{\cdot}5H_2O$ under magnetic stirring. Then, the solution was transferred into a 25 mL beaker in a Teflon-lined stainless steel autoclave and heat treated at 180°C for 6 h. After reaction, the autoclave was left to cool down to room temperature. The products were centrifuged and collected. Then, the products were washed for several times with deionized water and ethanol. In the end, the ZrO_2 products were obtained by drying at 90°C for 8 h.

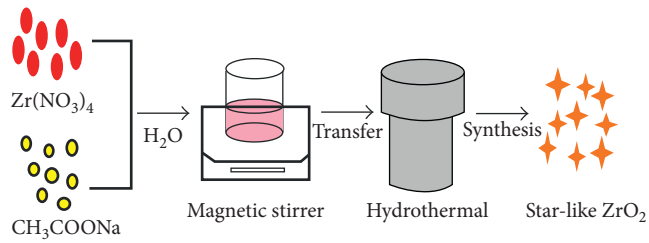

Figure 1: Flowchart of the preparation route of star-like ZrO_2.

2.3. Characterization. The morphology was investigated using the high-resolution transmission electron microscope (HR-TEM, Tecnai G2 F20) working with an accelerating voltage of 200 kV. The phase constitution of the products were analyzed by an X-ray diffractometer (Rigaku D/M4X 2500, Rigaku Co., Japan) with Cu Kα radiation ($\lambda = 0.15418$ Å). The infrared (FTIR) spectra were measured by a Nicolet is 35 using the KBr pellet technique in the range of 4000–400 cm^{-1}. Thermogravimetric (TG) analysis was recorded on a Netzsch STA 449 F3 at a heating rate of 10°C·min^{-1} in a flowing air. The UV-visible spectrum of ZrO_2 was measured using the Cary 300 UV-visible spectrophotometer. The X-ray photoelectron spectrum (XPS) was recorded on an ESCALAB 250Xi spectrometer with an energy analyzer working in the pass energy mode at 20.0 eV, and the Al Kα line was used as the excitation source. The binding energy reference was taken at 284.8 eV for the C1s peak arising from surface hydrocarbons. Brunauer–Emmett–Teller (BET) surface area was obtained with N_2 adsorption by using a Micromeritics ASAP 2020 nitrogen adsorption apparatus via determination of nitrogen adsorption isotherm at 77 K.

2.4. Photocatalytic Activity Test. The photocatalytic experiments were carried out by following the RhB degradation under UV irradiation in a separate chamber. Prior to irradiation, the suspensions were magnetically stirred in a complete darkness for 20 min to attain adsorption equilibrium. During the RhB photodecomposition, the samples were withdrawn at regular intervals and centrifuged to separate solid particles for analysis. The concentration of RhB was determined by a UV-Vis spectroscopy at its maximum absorption wavelength (about 554 nm).

3. Results and Discussion

3.1. Characterizations of ZrO_2 Nanostructures. The XRD results of the products, prepared at 180°C with different reaction times, are shown in Figure 2. It can be seen that the

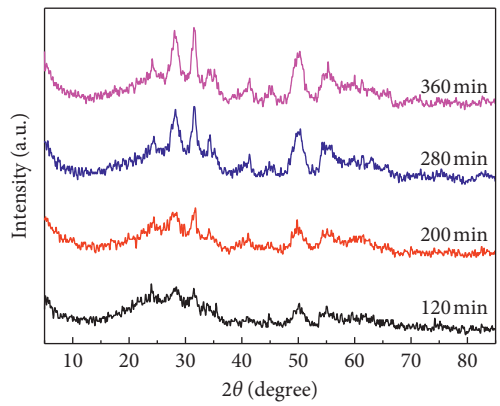

Figure 2: XRD patterns of the products prepared at different reaction times.

product heat treated for 120 min was crystalline, but the peaks were not sharp. The onset of monoclinic ZrO_2 was observed in the product heat treated for 200 min. The crystallinity of the products increased with the reaction time. When the hydrothermal time was prolonged to 360 min, the products changed into monoclinic ZrO_2 completely (JCPDS number 37–1484), and no other phase was observed.

The mean crystallite size of the products was calculated by the following Scherrer equation:

$$\tau = \frac{k\lambda}{\beta \cos\theta}, \quad (1)$$

where τ is the mean size, k is the shape factor, β is the full width at half the maximum (FWHM) intensity, θ is the Braggs angle, and λ is the wavelength of X-ray source applied in XRD. The calculated average crystallite size of ZrO_2 at 120 min reaction time was 6.97 nm. When the reaction time was 360 min, the crystallite size of ZrO_2 was found to be approximately 9.02 nm (Table 1). These results suggest that the crystallite size of ZrO_2 increases with increasing reaction time. The small crystallite size of ZrO_2 may be due to the groups adsorbed on the surface as well as on the grain boundary. These adsorbed groups may prevent the continuous growth of zirconium oxide nanocrystals, which can be achieved by reducing their surface energy and surface activity.

The morphologies of ZrO_2 were investigated by FE-SEM and TEM. From Figures 3(a) and 3(b), it can be seen that ZrO_2 exhibited a beautiful star-like shape, and stars were in the range of 30–80 nm. The HR-TEM image in Figure 3(c) shows that ZrO_2 stars were composed of short nanorods of ca. 15–20 nm in length and 3–5 nm in diameter. The corresponding selected area electron diffraction (SAED) pattern of a single structure is a ring pattern (Figure 3(d)), suggesting that ZrO_2 has a short-range crystalline structure on the nanoscale. The HR-TEM image shown in Figure 3(f) is the magnification at the area denoted by the black arrow in Figure 3(e). The lattice fringe with an interplanar spacing of 0.28 nm is consistent with the value of the (111) lattice planes of ZrO_2 (JCPDS number 37-1484).

Figure 4(a) presents the FTIR spectrum of the star-like ZrO_2. The absorption bands at 751 cm^{-1}, 679 cm^{-1}, and 504 cm^{-1} are assigned to the vibration of Zr-O [36]. The absorption bands between 1000 and 1400 cm^{-1} are due to NO_3^- anions. However, nitrate groups were no longer coordinated in a chemical bond fashion, and nitrate anions only remained on the ZrO_2 nanostructure surface. The absorption at 1531 cm^{-1} is due to the symmetric vibration absorption of COO^- [15]. The bands at 3234 cm^{-1} and 1638 cm^{-1} are attributed to the surface hydroxyl groups or adsorbed water strongly bound to the ZrO_2 surfaces [37]. It is reported that surface hydroxyl groups play an important role in heterogeneous photocatalysis and act by capturing light-induced holes thereby, producing reactive hydroxyl radicals with high oxidation capacity [38, 39]. This result suggests that the surface of ZrO_2 was probably covered by acetate groups, hydroxyl, and adsorbed water.

Table 1: Estimated crystallite sizes of ZrO_2 synthesized at different reaction times.

Sample	Crystal face	FWHM (rad)	Crystallite size (nm)
ZrO_2 (120 min)	[−1 1 1]	0.0215	6.97
ZrO_2 (200 min)	[−1 1 1]	0.0205	7.31
ZrO_2 (280 min)	[−1 1 1]	0.0182	8.23
ZrO_2 (360 min)	[−1 1 1]	0.0166	9.02

XPS measurements were performed on the product (Figure 4(b)), and the signals of Zr, O, C, and N were detected in the survey XPS of ZrO_2. The signals at 181.6 and 183.9 eV correspond to Zr3d5/2 and Zr3d3/2 of ZrO_2 (Figure 4(c)), which are found to be those related to the presence of zirconium in the composite, that is, Zr^{4+} of ZrO_2 as reported in [40]. The O1s peaks at 529.4, 531.1, and 532.4 eV can be ascribed to the lattice oxygen, the adsorbed oxygen (–OH, H_2O), and acetate groups, respectively [41] (Figure 4(d)). The high-resolution C1s XPS of ZrO_2 shows a strong peak at 284.2 eV, which can be attributed to C-C, and another relatively weak C1s peak is also observed, which can be ascribed to –COOH adsorbed on the surface of ZrO_2 in the form of acetate [42] (Figure 4(e)). In addition, Figure 4(f) shows a weak N1s peak at 406.6 eV, which may result from a small amount of residual nitrate as confirmed by checking the binding energy table [42]. According to literature results [43], XPS peaks of N in N-doped ZrO_2 are at 396.8 eV(Zr-N) and 400.0eV (N-O), respectively. Therefore, there is no nitrogen doping in the as-prepared ZrO_2 (406.6 eV) (Figure 4(f)). The XPS results indicate that the sample possesses a surface-adsorbed water, hydroxyl, and acetate groups, which is consistent with the FTIR spectra.

The TG curve of the ZrO_2 product is shown in Figure 5. The TG curve shows three-stage weigh loss events at 25–165°C, 165–500°C, and 500–1200°C, respectively. There is ca. 1.94% weight loss upon heating from room temperature to 165°C, which is due to the removal of adsorbed water on the surface of the product. The weight loss from 165°C to 500°C may be ascribed to the decomposition of the CH_3COO^- and NO_3^- anions, as the acetate and nitrate anions generally combust at about 350°C [44] and 192°C [45], respectively. The weight loss between 500°C and 1200°C is a result of the elimination of hydroxyls adsorbed

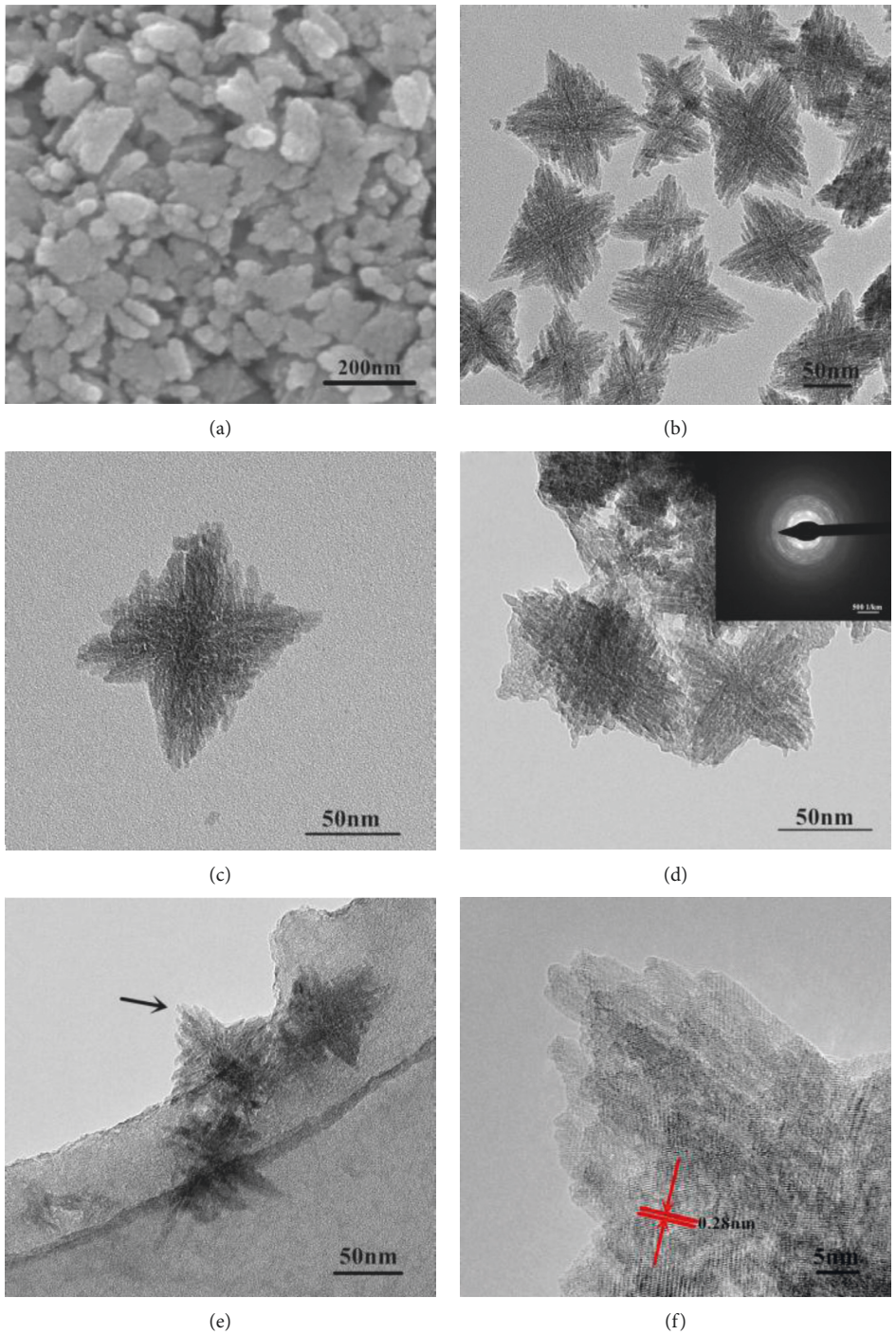

Figure 3: SEM image (a), TEM image (b, c), SAED patterns (d), TEM image (e) of the synthesized ZrO_2, and (f) HR-TEM image of the area denoted by the black arrow in (e).

on the surface. From the analysis of the TG curve and IR spectrum, the final product is covered by adsorbed water, CH_3COO^-, NO_3^-, and hydroxyl, respectively. However, it was difficult to analyze the TG curve quantitatively due to the overlap of the weight loss.

3.2. Photocatalytic Activities of ZrO_2. The degradation of RhB under UV irradiation was carried out to evaluate the photocatalytic activity of as-prepared ZrO_2 nanostructures. For comparison, a blank experiment without catalyst was also conducted under identical conditions. Figure 6(a) indicates that the RhB concentration decreases with increasing irradiation time. When the solution was irradiated for 30 min without catalyst, a small amount of RhB was degraded (<20%). This result is similar to the results reported by other authors [24]. When the as-prepared star-like ZrO_2 was added into the solution, the degradation of RhB increased

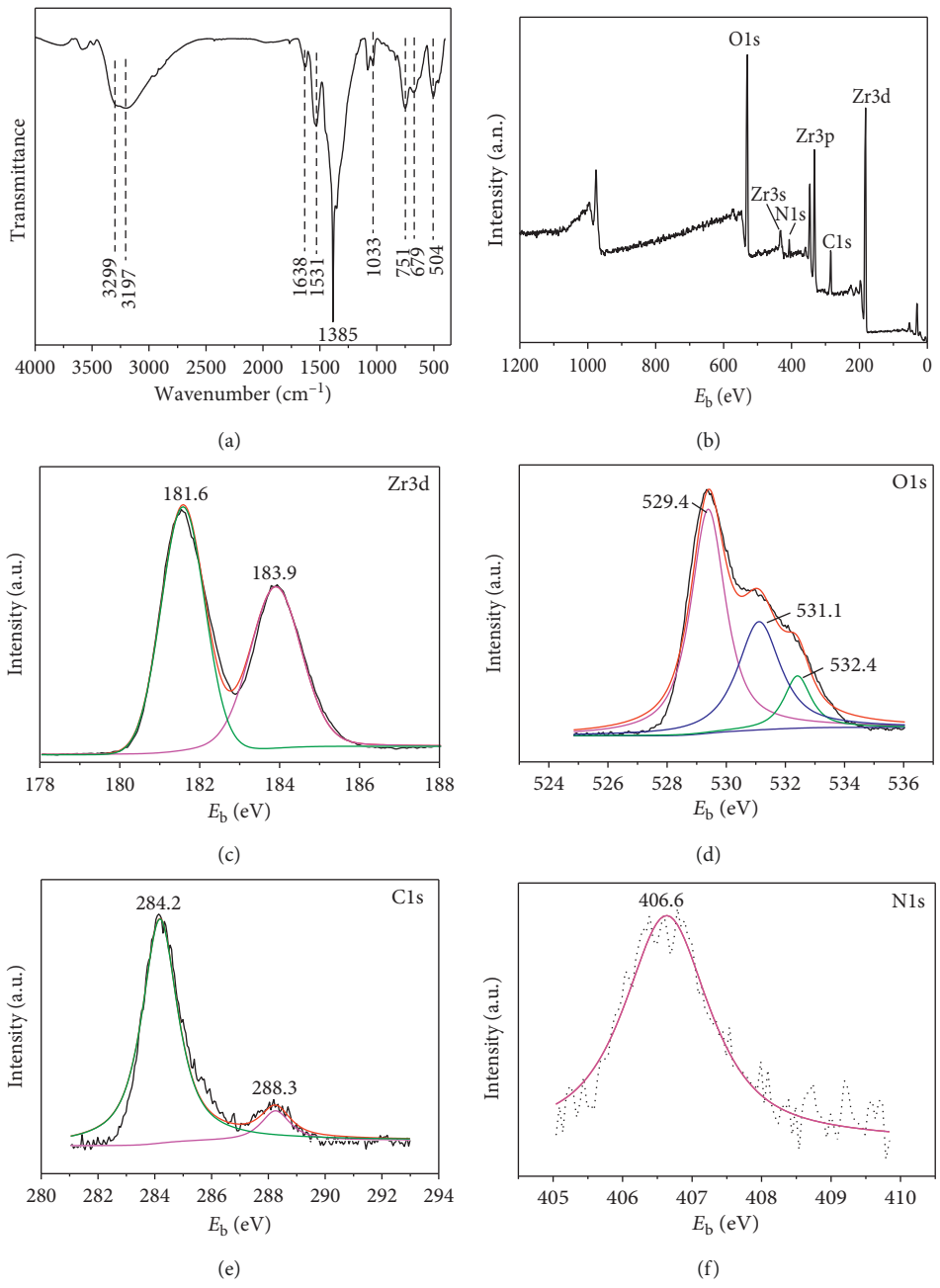

Figure 4: FTIR (a) and XPS (b–f) results showing the survey spectra of ZrO_2 products.

up to nearly 100% in 30 min, which shows an improved photocatalytic activity compared to the previous reports [24] (RhB degradation 100% in 40 min with flower-like ZrO_2). All products synthesized with different molar ratios of Zr $(NO_3)_4{\cdot}5H_2O$ to CH_3COONa showed a superior photocatalytic performance (Figure 6(b)).

The excellent photocatalytic activity of star-like ZrO_2 nanostructures can be attributed to several factors. Firstly, the star-like nanostructures may provide more adsorption sites and stronger surface adsorption ability to the RhB molecules, so the photocatalytic reaction can take place efficiently. Secondly, the improved surface functions may also contribute to the high photocatalytic activity of catalysts. To confirm this suggestion, the as-prepared star-like ZrO_2 was calcined (C-ZrO_2) at 600°C for 2 h and used as the catalyst at the same condition. It was found that only 60% of the RhB degraded after irradiation for 30 min with the calcined ZrO_2 as shown in Figure 6(a). Compared with the as-prepared ZrO_2, the as-calcined ZrO_2 showed a decreased photocatalytic activity toward the degradation of RhB. Furthermore, the FTIR was used to characterize the surface-adsorbed groups of ZrO_2 (Figure 7). It can be seen that the intensity of OH (3246 cm^{-1} and 1632 cm^{-1}) and NO_3^- absorption bands (1384 cm^{-1}) of calcined ZrO_2 at 600°C was significantly reduced compared to that of as-prepared ZrO_2. Furthermore, the vibration absorption bands of acetate groups completely disappeared after

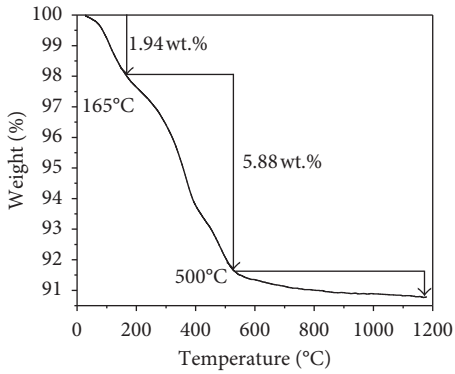

Figure 5: TG curve of ZrO_2 products obtained by reacting at 180°C for 6 h.

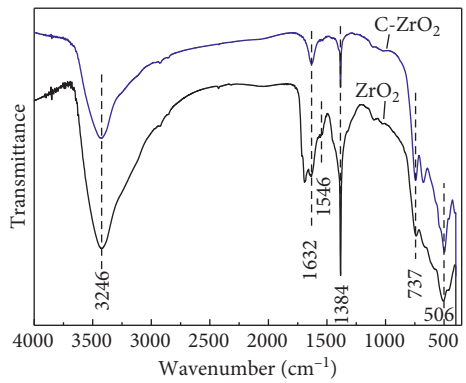

Figure 7: FTIR of the nanosized ZrO_2 and ZrO_2 calcined at 600°C.

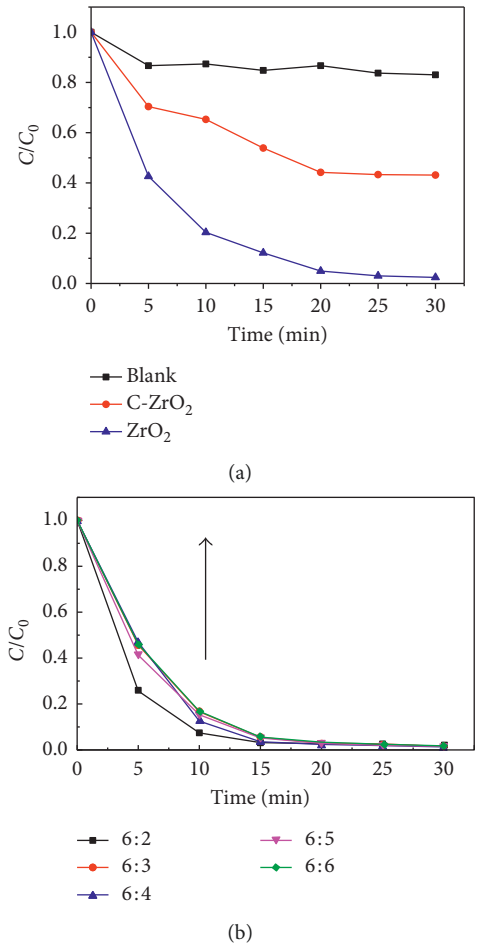

Figure 6: RhB concentration as a function of UV irradiation time over the product and calcined ZrO_2 (a) and the products with different molar ratios (b).

calcination. This indicates that the surface-adsorbed groups (hydroxyl or acetate groups) of the star-like ZrO_2 were destroyed during calcination and the surface chemistry of ZrO_2 changed. The acidity comes from hydroxyl groups since they capture light-induced holes [46], thereafter initiating the generation of strong active species (e.g., ·OH), capable of oxidizing adsorbed organic substrates [47]. Thus, the surface-adsorbed hydroxyl groups or water plays an important role in the high photocatalytic activity of star-like ZrO_2. Finally, to further probe the reason of the superior catalytic property of ZrO_2, the UV-Vis adsorption spectra of ZrO_2 and ZrO_2 calcined at 600°C for 2 h were measured (Figure 8(a)). It can be seen from Figure 8(a) that all star-like ZrO_2 showed a strong absorption in UV-Vis region with the maximum intensity at 300 nm, and an absorption band was also found at 348 nm. The absorption of the calcined ZrO_2 was, on the contrary, much weaker, and a considerable shift towards lower wavelength was found. For the obtained UV-Vis spectra, a bandgap was calculated using the Kubelka–Munk theory and Tauc method. The following equation was used to calculate the bandgap:

$$(Ahv)^2 = K\left(hv - E_g\right), \tag{2}$$

where A is the absorbance, K is the proportionality constant, and E_g is the bandgap energy. The plot of $(Ahv)^2$ versus hv based on the direct transition is shown in Figure 8(b). The measured bandgap for the as-prepared ZrO_2 was found to be 3.56 eV, while the calcined ZrO_2 exhibited a wide bandgap of 5.22 eV. In our experiments, the bandgap of synthesized star-like ZrO_2 with various molar ratios of $Zr(NO_3)_4{\cdot}5H_2O$ to CH_3COONa was in the range of 3.50–3.85 eV, according to the results of UV-Vis spectra (Figures 9(a) and 9(b)). The narrow bandgap of the synthesized star-like ZrO_2 nanostructures could also relate to its surface functions and contribute to the superior photocatalytic activity.

The N_2 adsorption-desorption isotherm plots for the as-prepared ZrO_2 and the as-calcined ZrO_2 at 600°C are shown in Figure 10. Both samples exhibited type IV isotherms, indicating a typical mesoporous structure. The BET specific surface area of the as-prepared ZrO_2 was approximately 70.9 m^2/g (Figure 10(a)), which is higher than that of ZrO_2 calcined at 600°C. The ZrO_2 calcined at 600°C showed a smaller BET specific surface area of 26.5 m^2/g (Figure 10(b)), which indicates that the BET specific surface area of ZrO_2 decreased with calcining at 600°C. This may be another reason for the decreased photocatalytic activity towards the degradation of RhB by calcined ZrO_2.

As reported in the literature, when the solid material is irradiated with ultraviolet light, some holes are left in the

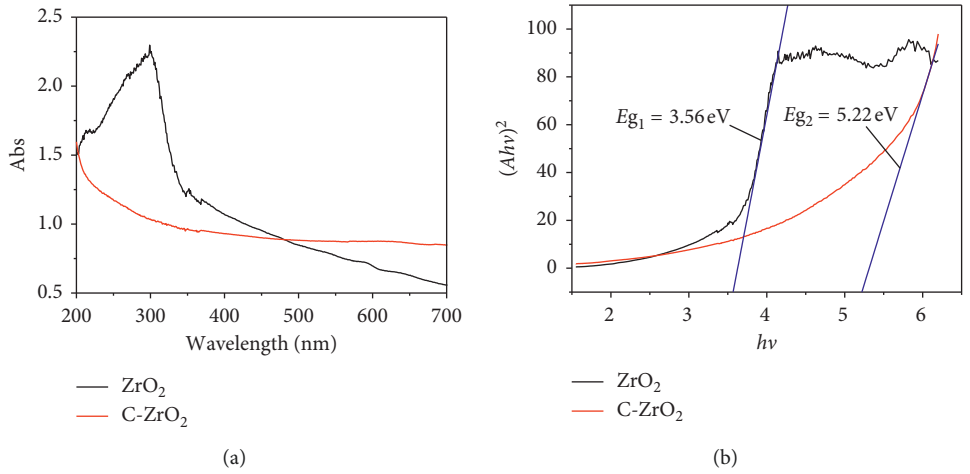

FIGURE 8: (a) UV-visible adsorption spectra of the nanosized ZrO_2 and the calcined ZrO_2; (b) plot of transformed Kubelka–Munk function versus light energy for different samples.

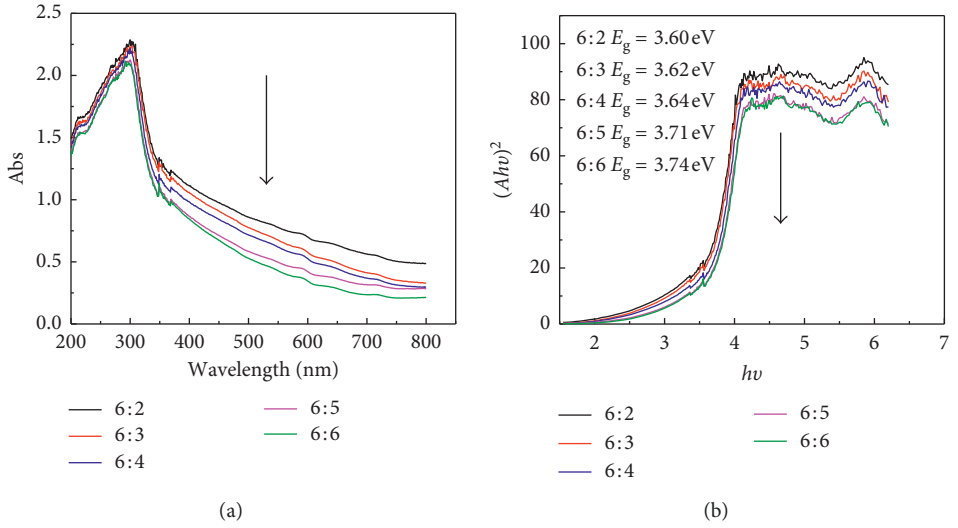

FIGURE 9: (a) UV-visible adsorption spectra of the star-like ZrO_2 with various molar ratios of $Zr(NO_3)_4{\cdot}5H_2O$ to CH_3COONa; (b) plot of transformed Kubelka–Munk function versus the energy of light for different samples.

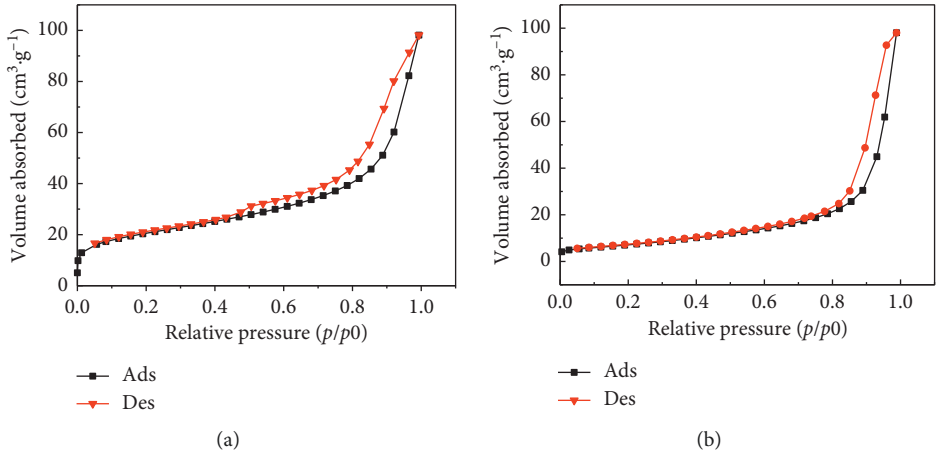

FIGURE 10: N_2 adsorption-desorption isotherms of (a) star-like ZrO_2 and (b) ZrO_2 calcined at 600°C.

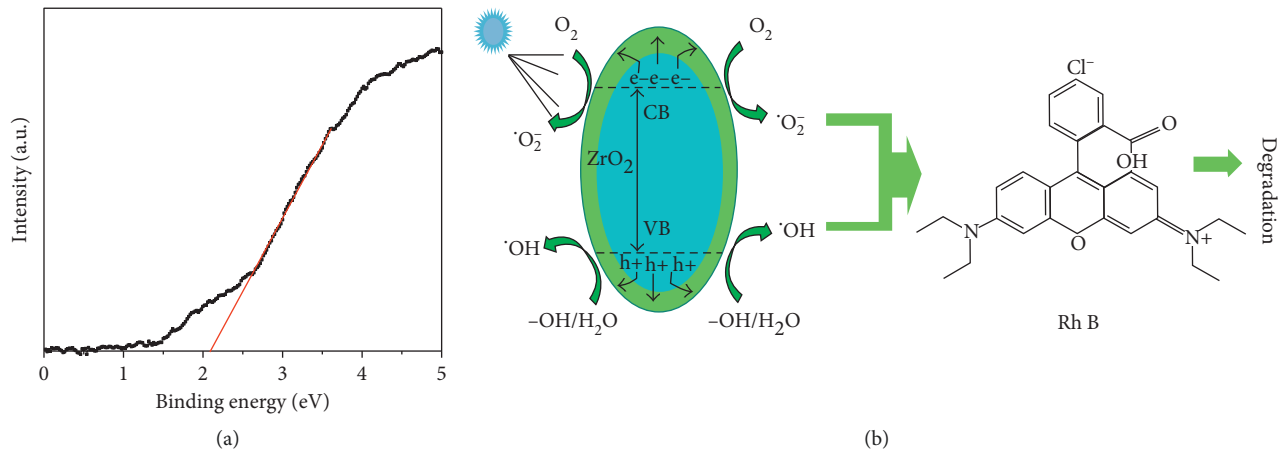

FIGURE 11: (a) Valence band (VB) XPS of the prepared ZrO_2 and (b) possible photocatalytic mechanism scheme with as-prepared ZrO_2 nanostructures.

valence band along with the process of electron transition from the valence band to the conduction band [48]. The photogenerated electrons and holes are the origin of the photocatalytic reaction. The results of the valence band (VB) XPS showed that the valence band energy of prepared ZrO_2 was 2.08 eV (Figure 11(a)). The optical bandgap energy of prepared ZrO_2 was 3.56 eV. According to the relationship $E_{VB} = E_{CB} + E_g$, the conduction band (CB) of prepared ZrO_2 would occur at −1.48 eV. Because the CB edge potential of ZrO_2 is more negative than $E^{\cdot}_{O_2/O_2}$ (−0.046 V) [49], the electrons in ZrO_2 can capture O_2 and reduce it to $^{\cdot}O_2^-$, which could effectively suppress the electron-hole recombination rates [50]. Meanwhile, the holes are captured by OH groups or H_2O on the surface of ZrO_2 to produce hydroxyl radicals. Finally, the radicals formed, such as superoxide and hydroxyl, react with the RhB and degrade it completely. The abovementioned reactions take place on the surface of ZrO_2 with a high efficiency. The radicals produced react powerfully in the RhB solution and cause their degradation. The possible mechanism may be described as follows:

$$\begin{aligned} ZrO_2 + h\nu &\longrightarrow h^+ + e^- \\ h^+ + e^- &\longrightarrow \text{energy} \\ O_2 + e^- &\longrightarrow {}^{\cdot}O_2^- \\ OH + h^+ &\longrightarrow {}^{\cdot}OH \\ H_2O + h^+ &\longrightarrow H^+ + {}^{\cdot}OH \\ {}^{\cdot}O_2^- + \text{RhB} &\longrightarrow \text{degradation} \\ {}^{\cdot}OH + \text{RhB} &\longrightarrow \text{degradation} \end{aligned} \tag{3}$$

Sudrajat and Babel [43] studied the mechanism of nitrogen-doped ZrO_2-catalyzed degradation of rhodamine 6G. They found that·OH was the most dominant reactive species. The photogenerated h^+ also seems to play an important role in the dye degradation through direct attack of R6G molecules on the catalyst surface. $^{\cdot}O_2^-$ is more easily produced through reduction of O_2 by the electron in the CB of N-ZrO_2 due to high CB potential of N-ZrO_2. Other references present a similar reaction mechanism. Combining the above presented results with the literature reports, the possible photodegradation mechanism can be inferred (Figure 11(b)). In all the cases, the role of photogenerated electrons is negligible. This is an indication of an effective electron transfer from the catalyst surface to the adsorbed molecules to produce reactive species [43].

4. Conclusions

To sum up, the synthesis of star-like ZrO_2 nanostructures has been successfully carried out by using the hydrothermal method without any template and surfactant. The crystallite size of ZrO_2 increased with increasing reaction time, and the crystallite size was approximately 9.02 nm when the reaction time was 360 min. The FTIR and XPS spectra showed the surface of ZrO_2 was covered by acetate groups, hydroxyl, and adsorbed water. The bandgap of the as-synthesized star-like ZrO_2 with various molar ratios of $Zr(NO_3)_4{\cdot}5H_2O$ to CH_3COONa was in the range of 3.50–3.85 eV, according to the results of UV-Vis spectroscopy. The as-synthesized nano-ZrO_2 showed excellent photocatalytic activities in RhB degradation under UV irradiation which may be attributed to the surface functions, special morphology, and narrow bandgap of the star-like ZrO_2 nanostructures. The possible photodegradation mechanism was proposed, and potential applications of the synthesized star-like ZrO_2 have been considered. Reactive species·OH and $^{\cdot}O_2^-$ may play an important role in the RhB degradation. Overall, the star-like ZrO_2 nanostructures have been proven to be effective catalysts for the degradation of RhB under UV-Vis radiation and could be suitable candidates in environmental photocatalysis.

Data Availability

The data used to support the findings of this study are available from the corresponding author upon request.

Conflicts of Interest

The authors declare that they have no conflicts of interest.

Acknowledgments

This research was supported by "the Fundamental Research Funds for the Central Universities" (Grant no. 2015 QNA07).

References

[1] G. Busca, *Heterogeneous Catalytic Materials: Solid State Chemistry, Surface Chemistry and Catalytic Behaviour*, Elsevier, New York, NY, USA, 2014.

[2] D. Ciuparu, A. Ensuque, G. Shafeev, and F. Bozon-Verduraz, "Synthesis and apparent bandgap of nanophase zirconia," *Journal of Materials Science*, vol. 19, no. 11, pp. 931–933, 2000.

[3] G. Poungchan, B. Ksapabutr, and M. Panapoy, "One-step synthesis of flower-like carbon-doped ZrO_2 for visible-light-responsive photocatalyst," *Materials Design*, vol. 89, pp. 137–145, 2016.

[4] A. R. Ardiyanti, A. Gutierrez, M. L. Honkela, A. O. I. Krause, and H. J. Heeres, "Hydrotreatment of wood-based pyrolysis oil using zirconia-supported mono- and bimetallic (Pt, Pd, Rh) catalysts," *Applied Catalysis A: Generation*, vol. 407, no. 1-2, pp. 56–66, 2011.

[5] S. Guerrero, P. Araya, and E. E. Wolf, "Methane oxidation on Pd supported on high area zirconia catalysts," *Applied Catalysis A: Generation*, vol. 298, pp. 243–253, 2006.

[6] S. Tekeli, "The solid solubility limit of Al_2O_3 and its effect on densification and microstructural evolution in cubic-zirconia used as an electrolyte for solid oxide fuel cell," *Materials Design*, vol. 28, no. 2, pp. 713–716, 2007.

[7] Y. W. Suh, J. W. Lee, and H. K. Rhee, "Synthesis of thermally stable tetragonal zirconia with large surface area and its catalytic activity in the skeletal isomerization of 1-butene," *Catalysis Letters*, vol. 90, no. 1-2, pp. 103–109, 2003.

[8] V. V. Brei, "Superacids based on zirconium dioxide," *Theoretical and Experimental Chemistry*, vol. 47, no. 3, pp. 165–175, 2005.

[9] S. Samantaray, B. G. Mishra, D. K. Pradhan, and G. Hota, "Solution combustion synthesis and physicochemical characterization of ZrO_2-MoO_3 nanocomposite oxides prepared using different fuels," *Ceramics International*, vol. 37, no. 8, pp. 3101–3108, 2011.

[10] Y. Lu, Z. Wang, S. Yuan, L. Shi, Y. Zhao, and W. Deng, "Microwave-hydrothermal synthesis and humidity sensing behavior of ZrO_2 nanorods," *RSC Advances*, vol. 3, no. 29, pp. 11707–11714, 2013.

[11] M. Habulan, "Deposition of sol-gel ZrO_2 films on stainless steel," *Evolution*, vol. 57, pp. 2904–2910, 2014.

[12] P. Murugavel, M. Kalaiselvam, A. R. Raju, and C. N. R. Rao, "Sub-micrometre spherical particles of TiO_2, ZrO_2 and PZT by nebulized spray pyrolysis of metal-organic precursors," *Journal of Materials Chemistry*, vol. 7, no. 8, pp. 1433–1438, 2015.

[13] T. S. Jeon, J. M. White, and D. L. Kwong, "Thermal stability of ultrathin ZrO_2 films prepared by chemical vapor deposition on Si(100)," *Applied Physics Letters*, vol. 78, no. 3, pp. 368–370, 2001.

[14] X. Dong, Z. Liu, J. Yan, J. Wang, and G. Hong, "Preparation of nanocrystalline ZrO_2 by reverse precipitation method," *Journal of Wuhan University of Technology*, vol. 20, no. 3, pp. 1–4, 2005.

[15] Z. Shu, X. Jiao, and D. Chen, "Hydrothermal synthesis and selective photocatalytic properties of tetragonal star-like ZrO_2 nanostructures," *CrystEngComm*, vol. 15, no. 21, pp. 4288–4294, 2013.

[16] E. Beltowska-Lehman, P. Indyka, A. Bigos, M. J. Szczerba, and M. Kot, "Ni-W/ZrO_2 nanocomposites obtained by ultrasonic DC electrodeposition," *Materials Design*, vol. 80, pp. 1–11, 2015.

[17] Q. X. Gao, X. F. Wang, X. C. Wu, Y. R. Tao, and J. J. Zhu, "Mesoporous zirconia nanobelts: preparation, characterization and applications in catalytical methane combustion," *Microporous and Mesoporous Materials*, vol. 143, no. 2-3, pp. 333–340, 2011.

[18] H. Q. Cao, X. Q. Qiu, B. Luo et al., "Synthesis and room-temperature ultraviolet photoluminescence properties of zirconia nanowires," *Advanced Functional Material*, vol. 14, no. 3, pp. 243–246, 2004.

[19] H. M. Abdellaal, "One-pot path for the synthesis of hollow zirconia sub-microspheres using hydrothermal approach," *Materials Letters*, vol. 212, pp. 218–220, 2018.

[20] J. L. Gole, S. M. Prokes, J. D. Stout, O. J. Glembocki, and R. Yang, "Unique properties of selectively formed zirconia nanostructures," *Advanced Materials*, vol. 18, no. 5, pp. 664–667, 2006.

[21] B. B. Nayak, S. K. Mohanty, M. Q. B. Takmeel, D. Pradhan, and A. Mondal, "Borohydride synthesis and stabilization of flake-like tetragonal zirconia nanocrystallites," *Materials Letters*, vol. 64, no. 17, pp. 1909–1911, 2010.

[22] A. M. Azad, "Fabrication of yttria-stabilized zirconia nanofibers by electrospinning," *Materials Letters*, vol. 60, no. 1, pp. 67–72, 2006.

[23] J. B. Joo, A. Vu, Q. Zhang, M. Dahl, M. Gu, and F. Zaera, "A sulfated ZrO_2 hollow nanostructure as an acid catalyst in the dehydration of fructose to 5-hydroxymethylfurfural," *ChemSusChem*, vol. 6, no. 10, pp. 2001–2008, 2013.

[24] Z. Shu, X. Jiao, and D. Chen, "Synthesis and photocatalytic properties of flower-like zirconia nanostructures," *CrystEngComm*, vol. 14, no. 3, pp. 1122–1127, 2012.

[25] X. Yang, X. Song, Y. Wei, W. Wei, L. Hou, and X. Fan, "Synthesis of spinous ZrO_2 core-shell microspheres with good hydrogen storage properties by the pollen bio-template route," *Scripta Materialia*, vol. 64, no. 12, pp. 1075–1078, 2011.

[26] T. F. Ma, J. Bai, and C. P. Li, "Facile synthesis of g-C_3N_4 wrapping on one-dimensional carbon fiber as a composite photocatalyst to degrade organic pollutants," *Vacuum*, vol. 145, pp. 47–54, 2017.

[27] P. Supriya, B. T. V. Srinivas, K. Chowdeswari, N. V. S. Naidu, and B. Sreedhar, "Biomimetic synthesis of gum acacia mediated Pd-ZnO and Pd-TiO_2-promising nanocatalysts for selective hydrogenation of nitroarenes," *Materials Chemistry and Physics*, vol. 204, pp. 27–36, 2017.

[28] Z. Liu, Q. Zhang, Y. Li, and H. Wang, "Solvothermal synthesis, photoluminescence and photocatalytic properties of pencil-like ZnO microrods," *Journal of Physics and Chemistry of Solids*, vol. 73, no. 5, pp. 651–655, 2012.

[29] N. F. Jaafar, A. A. Jalil, S. Triwahyono, M. N. M. Muhid, N. Sapawe, and M. A. H. Satar, "Photodecolorization of methyl orange over α-Fe_2O_3-supported HY catalysts: the effects of catalyst preparation and dealumination," *Chemical Engineering Journal*, vol. 191, pp. 112–122, 2012.

[30] J. Zhang, L. Li, and D. Liu, "Multi-layer and open three-dimensionally ordered macroporous TiO_2-ZrO_2 composite: diversified design and the comparison of multiple mode photocatalytic performance," *Materials Design*, vol. 86, pp. 818–828, 2015.

[31] A. Nezamzadeh-Ejhieh and M. Karimi-Shamsabadi, "Decolorization of a binary azo dyes mixture using CuO incorporated nanozeolite-X as a heterogeneous catalyst and solar irradiation," *Chemical Engineering Science*, vol. 228, pp. 631–641, 2013.

[32] C. Suciu, L. Gagea, A. C. Hoffmann, and M. Mocean, "Sol-gel production of zirconia nanoparticles with a new organic precursor," *Chemical Engineering Science*, vol. 61, no. 24, pp. 7831–7835, 2006.

[33] J. Zhao, X. Wang, L. Zhang, X. Hou, Y. Li, and C. Tang, "Degradation of methyl orange through synergistic effect of zirconia nanotubes and ultrasonic wave," *Journal of Hazardous Materials*, vol. 188, no. 1–3, pp. 231–234, 2011.

[34] L. Renuka, K. S. Anantharaju, S. C. Sharma et al., "Hollow microspheres Mg-doped ZrO_2 nanoparticles: green assisted synthesis and applications in photocatalysis and photoluminescence," *Journal of Alloys and Compounds*, vol. 672, pp. 609–622, 2016.

[35] L. Xu and H. K. Lee, "Zirconia hollow fiber: preparation, characterization, and microextraction application," *Analytic Chemistry*, vol. 79, no. 14, pp. 5241–5248, 2007.

[36] D. V. Pinjari, K. Prasad, and P. R. Gogate, "Intensification of synthesis of zirconium dioxide using ultrasound: effect of amplitude variation," *Chemical Engineering and Process*, vol. 74, pp. 178–186, 2013.

[37] A. Brisdon and K. Nakamoto, "Infrared and Raman spectra of inorganic and coordination compounds, part B, applications in coordination, organometallic, and bioinorganic chemistry," *Applied Organometallic Chemistry*, vol. 24, p. 489, 2010.

[38] A. Manikandan, L. J. Kennedy, and J. J. Vijaya, "Comparative investigation of zirconium oxide ($ZrO_{(2)}$) nano and microstructures for structural, optical and photocatalytic properties," *Journal of Colloid and Interface Science*, vol. 389, pp. 91–98, 2013.

[39] X. Fu., L. A. Clark, and Q. Yang, "Enhanced photocatalytic performance of titania-based binary metal oxides: TiO_2/SiO_2 and TiO_2/ZrO_2," *Environmental Science and Technology*, vol. 30, no. 2, pp. 647–653, 1996.

[40] J. Zhang, L. Li, Z. Xiao, D. Liu, S. Wang, and J. Zhang, "Hollow sphere TiO_2-ZrO_2 prepared by self-assembly with polystyrene colloidal template for both photocatalytic degradation and H_2 evolution from water splitting," *ACS Sustainable Chemistry and Engineering*, vol. 4, no. 4, pp. 2037–2046, 2016.

[41] A. V. Charanpahari, S. G. Ghugal, S. S. Umare, and S. Rajamma, "Mineralization of malachite green dye over visible light responsive bismuth doped TiO_2-ZrO_2 ferromagnetic nanocomposites," *New Journal of Chemistry*, vol. 39, no. 5, pp. 3629–3638, 2015.

[42] Z. Wang, Q. Long, L. Yuan, W. Zhang, X. Hu, and Y. Huang, "Functionalized N-doped interconnected carbon nanofibers as an anode material for sodium-ion storage with excellent performance," *Carbon*, vol. 55, pp. 328–334, 2013.

[43] H. Sudrajat and S. Babel, "Comparison and mechanism of photocatalytic activities of N-ZnO and N-ZrO_2 for the degradation of rhodamine 6G," *Environmental Science and Pollution Research*, vol. 23, no. 10, pp. 10177–10188, 2016.

[44] D. C. Perera, J. W. Hewage, and N. D. Silva, "Theoretical study of catalytic decomposition of acetic acid on MgO nanosurface," *Computational and Theoretical Chemistry*, vol. 1064, pp. 1–6, 2015.

[45] Y. Shanmugam, L. Fanyuan, C. Tsonghuei, and C. Yeh, "Thermal decomposition of metal nitrates in air and hydrogen environments," *Journal of Physical Chemistry B*, vol. 107, pp. 1044–1047, 2003.

[46] C. Anderson and A. J. Bard, "Improved photocatalytic activity and characterization of mixed TiO_2/SiO_2 and TiO_2/Al_2O_3 materials," *Journal of Physical Chemistry B*, vol. 101, no. 14, pp. 2611–2616, 1997.

[47] X. Chen, X. Wang, and X. Fu, "Hierarchical macro/mesoporous TiO_2/SiO_2 and TiO_2/ZrO_2 nanocomposites for environmental photocatalysis," *Energy & Environmental Science*, vol. 2, no. 8, pp. 872–877, 2009.

[48] L. Renuka, K. S. Anantharaju, S. C. Sharma et al., "A comparative study on the structural, optical, electrochemical and photocatalytic properties of ZrO_2 nanooxide synthesized by different routes," *Journal of Alloys and Compounds*, vol. 695, pp. 382–395, 2017.

[49] D. Wang, T. Kako, and J. Ye, "Efficient photocatalytic decomposition of acetaldehyde over a solid-solution perovskite $(Ag_{0.75}Sr_{0.25})$ $(Nb_{0.75}Ti_{0.25})O_3$ under visible-light irradiation," *Journal of the American Chemical Society*, vol. 130, no. 9, pp. 2724-2725, 2008.

[50] X. Wang, L. Zhang, H. Lin et al., "Synthesis and characterization of a ZrO_2/g-C_3N_4 composite with enhanced visible-light photoactivity for rhodamine degradation," *RSC Advances*, vol. 4, no. 75, pp. 29–35, 2014.